Japanese Journal of Applied Physics **55**, 04EA01 (2016)
http://doi.org/10.7567/JJAP.55.04EA01

REVIEW

Low-temperature solution processable n–i–p perovskite solar cell

Cheng-Ya Chu†, Chun-Yu Chang†, and Wei-Fang Su*

Department of Materials Science and Engineering, National Taiwan University, Taipei 10617, Taiwan

*E-mail: suwf@ntu.edu.tw
†These authors contributed equally to this work.

Received September 8, 2015; accepted November 16, 2015; published online February 26, 2016

Recently, the perovskite solar cells draw lots of attentions because of low cost, solution-processable and promising high efficiency. The power conversion efficiency (PCE) is rapidly reached to a certified value of 20.1%. However, the conventional electron transport layer (ETL) of the device needs to be sintered over 500 °C which is high energy-consumption process and cannot use on flexible substrate. Therefore, many research groups endeavor to develop low-temperature solution processable electron transport material in perovskite solar cells. In this review, we present systematic and critical discussions on the evolution of perovskite solar cells from meso-superstructure solar cells (MSSCs) to low-temperature solution processed planar heterojunction (PHJ) perovskite solar cells. This review will provide a guideline for the fabrication of high PCE perovskite solar cell using solution process at temperature of 150 °C or under, which has potential to achieve large scale fabrication by roll-to-roll technique for commercial products in near future.

1. Introduction

In human history, energy always plays an important role in the development of industries and societies. However, the limited reserve of fossil fuel and the risk of radiation leakage of nuclear power urge scientists to find sustainably alternative energy. Solar power is a promising alternative energy because it is inexhaustible and pollution-free. Recently, the organometallic trihalide perovskite solar cell has drawn a lot of attentions by the advantages of tunable absorption range,[1–11] high light absorption coefficient,[12–18] extremely high power conversion efficiency (PCE) of certified 20.1%[19] and low-temperature solution processability (<150 °C). The organometallic trihalide perovskite materials have the chemical formula of ABX_3 (A: organic cation; B: metal cation; X: halide, Cl, Br, or I). The optical and electrical properties can be controlled by changing the composition of A, B, or X. For example, it was reported that by substituting part of I by Cl, the mixed halide $CH_3NH_3PbI_{3-x}Cl_x$ perovskite has longer charge carriers diffusion length (over 1 μm) than the triiodide $CH_3NH_3PbI_3$ (about 100 nm).[20] In addition, by replacing the organic cation methylammonium $(CH_3NH_3)^+$ of $CH_3NH_3PbI_3$ with a larger formamidinium $[CH(NH_2)_2]^+$, the band gap can be tuned from 1.57 to 1.48 eV, which shows the structural-dependent property of the organometallic trihalide perovskite materials.[21]

The PCE of perovskite solar cell dramatically surged up from 3.81 to 20.1% in recent six years. In 2009, Miyasaka et al. first utilized the $CH_3NH_3PbI_3$ and $CH_3NH_3PbBr_3$ as the sensitizers in the dye sensitized solar cells (DSSCs) technology.[22] The device is composed with a TiO_2 mesoporous structure on a compact TiO_2 layer. The TiO_2 adsorbs the perovskite material and extracts out electrons at the same time. However, the device only achieved the PCE of 3.81%. In 2011, Park et al. demonstrated a perovskite quantum dot-sensitized solar cell[23] achieving the PCE of 6.20%, which outperformed the standard N719 dye-sensitized solar cell with much higher current density. However, the liquid electrolyte used here could easily dissolve the perovskite material and decrease the lifetime and stability of the devices. To solve this problem, Park et al. in 2012 developed an all sold-state perovskite-sensitized solar cell by replacing the liquid electrolyte with a small molecule 2,2′,7,7′-tetrakis(*N*,*N*-di-4-methoxyphenylamino)-9,9′-spirobifluorene (spiro-OMeTAD) as a hole transport material.[24] The PCE of the devices reached to 9.7% with a long term stability over 500 h.

As stated above, the n-type of TiO_2 mesoporous layer in "perovskite sensitized solar cell" can extract and transport electrons from perovskite material. However, Snaith et al. in 2012 replaced the TiO_2 mesoporous structure with Al_2O_3 mesoporous structure to fabricate a new device architecture with a PCE of 10.9% and open circuit voltage (V_{oc}) of 1.1 V.[25] Unlike TiO_2, the high energy band gap of Al_2O_3 (about 7 to 9 eV) restricts the transport of photon-induced electrons through Al_2O_3 mesoporous structure. The electrons can transport through the perovskite material itself to the compact TiO_2 layer and the Al_2O_3 is only served as a scaffold to adsorb the perovskite material. This type of solar cell with insulating mesoporous scaffold which is not involved in the electron transporting is called "meso-superstructure solar cells (MSSCs)". The MSSCs verifies that the n-type mesoporous material is not necessary in the perovskite based solar cell. Further remove the TiO_2 or Al_2O_3 mesoporous layer and leave only the compact TiO_2 layer to serve as electron transport layer (ETL) that creates the "planar heterojunction (PHJ) perovskite solar cells". This kind of solar cells significantly simplified the complicated process of fabricating the mesoporous layer without sacrificing the PCE.

Although the PCE of perovskite based solar cell has already surpassed the other thin film solar cells, the high-temperature sintering of high quality metal oxide ETL can damage the flexible substrate. Develop the low-temperature processable perovskite solar cell can extend the selection of transparent electrode. For example, indium tin oxides (ITO) is more conductive than fluorine doped tin oxide (FTO) at the temperature below about 200 °C, so it is more applicable in the low-temperature processing than FTO. Other solution processable transparent electrode such as silver nanowire, poly(3,4-ethylenedioxythiophene):poly(styrene sulfonate) (PEDOT:PSS), carbon nanotube or graphene can also be applied in the low-temperature processing. To date, many research groups are still working on the development of new low-temperature processable materials or new device architectures toward the roll-to-roll process which provides an easy and fast method to scale up the fabrication of the devices. For example, in 2014, Snaith et al. developed a new

Table I. Summary of electron transport layer fabrication temperature and the corresponding device performance in meso-superstructure solar cells.

Process temperature (°C) (compact layer/mesoporous scaffold)	Electron transport layer structure	V_{oc} (V)	J_{sc} (mA/cm^2)	FF (%)	PCE (%)	Ref.
500/500	ht-TiO_2/ms-Al_2O_3	0.98	17.8	0.63	10.9	25
500/500	ht-TiO_2/ms-Al_2O_3 + Au-doped SiO_2-NPs	1.02	16.9	0.64	11.4	28
500/500	ht-TiO_2/ms-Al_2O_3	1.50	4.0	0.46	2.7	29
450/550	ht-TiO_2/ms-Al_2O_3	1.30	1.08	0.40	0.6	30
500/150	ht-TiO_2/ms-Al_2O_3	1.02	22.7	0.66	15.3	31
500/150	ht-TiO_2/ms-Al_2O_3	1.02	18.0	0.67	12.3	33
500/150	ht-TiO_2/ms-Al_2O_3	1.08	18.3	0.60	11.9	32
150/150	TiO_2-NPs/ms-Al_2O_3	1.02	21.5	0.71	15.9	26
150/150	TiO_2-NPs-graphene/ms-Al_2O_3	1.04	21.9	0.73	16.6	34

method by using TiO_2 nanoparticles (TiO_2-NPs) to fabricate the compact TiO_2 layer with only 150 °C process temperature. The MSSCs fabricated with this method showed a high PCE of 15.9%.[26] In addition, Yang et al. utilized doping yttrium into TiO_2 nanoparticles to improve the conductivity of compact TiO_2 layer. Using other strategies such as using modifying the surface energy state of ITO by poly(ethylene imine) (PEIE) and fabricating the perovskite layer under controlled humidity, the device achieved a PCE of 19.3%,[27] which was the highest record with low temperature solution processable ETL represented in the literature.

In this review, we focus on the recent developments of low-temperature solution processed ETLs in MSSCs and n–i–p PHJ perovskite solar cells which have processing temperature at or under 150 °C. Different electron transport materials will be reviewed in detail. Finally, we conclude the review and provide some recommendations for the future development of low-temperature solution processed perovskite solar cells.

2. Development of electron transport layer in low-temperature solution processed n–i–p perovskite solar cell

There are two major types of low-temperature solution processed n–i–p structure perovskite solar cells: meso-superstructure and planar structure. The meso-superstructure consists of Al_2O_3-NPs mesoporous scaffold on a TiO_2 compact layer, which is termed MSSCs. On the other hand, the planar structure only consists of compact metal oxide ETL, such as TiO_2 and ZnO. In the following sections, the evolution of MSSCs from the origin high-temperature sintering process toward low-temperature solution processable devices is reviewed. Also, the low-temperature processed electron transport materials in PHJ perovskite solar cells is discussed.

2.1 Meso-superstructure solar cells

In the early stage, the Al_2O_3 mesoporous scaffold and compact layer of MSSCs were sintered over 500 °C.[28–30] However, some research groups successfully developed the new way to fabricate MSSCs at low temperature. The fabrication temperature of the device can be decreased to around 150 °C.[26,31–33] As a result, we summarize the fabrication temperature, device architecture and device performance of MSSCs that are reported in the literature and are showed in Table I.

The MSSCs were first introduced by the Snaith et al. in 2012.[25] In the perovskite sensitized solar cells system, the TiO_2 mesoporous structure is used to adsorb perovskite material and extract out electrons to the TiO_2 compact layer. However, due to the inappropriate energy level alignment, the electron transporting from perovskite material to TiO_2 mesoporous nanostructure causes an energy loss. The insulating property of Al_2O_3 in MSSCs blocks the electron transporting through the mesoporous structure. Figure 1(a) shows the schematic structure and cross-section scanning electron microscope (SEM) image of MSSCs. In this case, the Al_2O_3 meso-structure can only serve as a scaffold to adsorb perovskite material without participate the electron transporting, as shown in Fig. 1(b). Therefore, the perovskite material here not only functions as light absorber but also severs as electron transport material at the same time. The photon induced electrons in perovskite material diffuse through its whole layer to the TiO_2 compact layer. The transient photocurrent decay measurement even shows a faster electron transporting of MSSCs than the perovskite sensitized solar cells, as shown in Fig. 1(c). The reduced energy loss of electron transporting and faster electrons collection efficiency result in a high V_{oc} of 0.98 V and PCE of 10.9%.

Afterward, Snaith et al. found out the incorporation of core–shell Au-doped SiO_2-NPs into Al_2O_3 scaffold effectively improves the current density of device.[28] Because the absorption spectrum shows negligible difference between the device with and without core–shell NPs [Fig. 2(a)], the photoluminescence (PL) measurement is conducted for thorough investigation. The results show the presence of Au doped SiO_2-NPs significantly quench the PL, indicating a faster charge separation. Moreover, a temperature-dependent study of PL shows the binding energy of exciton is lowered after the incorporation of Au doped SiO_2-NPs. The enhanced incident photon-to-current efficiency (IPCE) also proves the improved generation of free charge carriers [Figs. 2(b) and 2(c)]. Finally the modified device can achieve the PCE of 11.4%.

The insulated Al_2O_3 scaffold mentioned above needs high-temperature sintering over 500 °C and it is an energy-consumption process. Therefore, Snaith et al. in 2013 reported a new method to construct the low-temperature mesoporous structure by Al_2O_3-NPs, which only needed the thermal annealing temperature at 150 °C and the devices can achieve the PCE of 12.3%.[33] At the same year, further improvement of the device architecture was conducted by

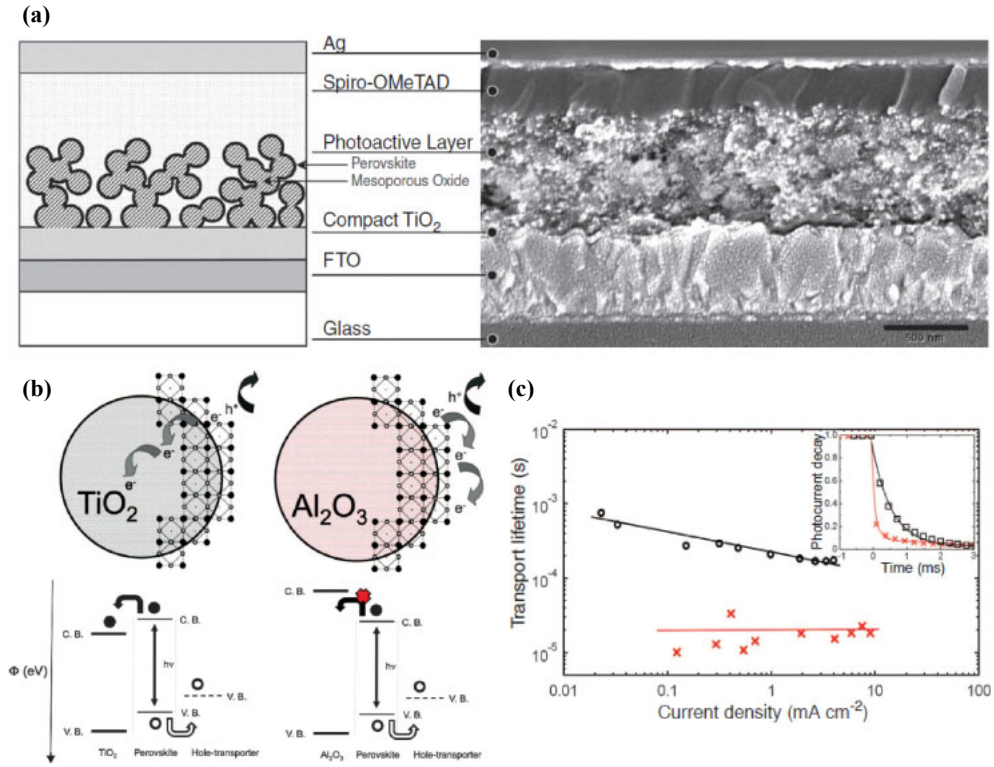

Fig. 1. (Color online) (a) Schematic structure and cross-section SEM image of MSSCs and (b) Electron transporting mechanism in TiO_2 mesoporous structure and Al_2O_3 meso-superstructure. (c) Charge transport lifetime and photocurrent decay are determined by small-perturbation transient photocurrent decay measurement for perovskite layer on TiO_2 meso-porous structure (black circles) and Al_2O_3 meso-structure (red crosses). Reprinted with permission from Ref. 25. © 2012 AAAS.

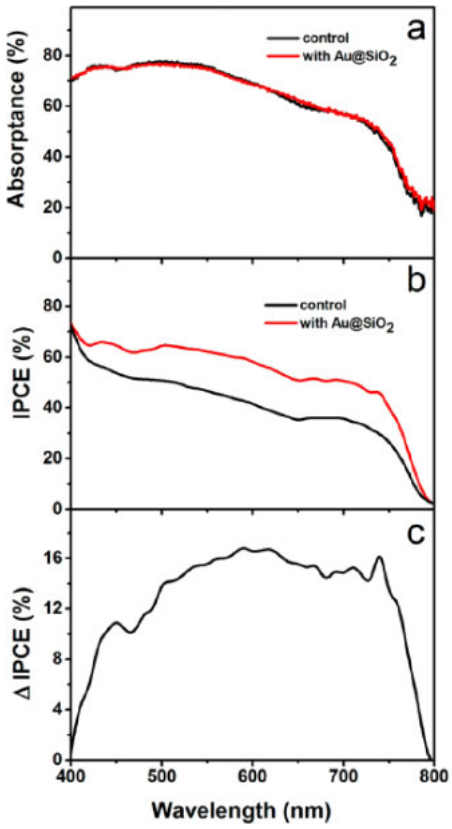

Fig. 2. (Color online) (a) Absorption spectrum of perovskite layer for the device without and with Au doped SiO_2-NPs. (b) ICPE spectrum of the device without and with Au doped SiO_2-NPs. (c) The increase of IPCE with the addition of Au doped SiO_2-NPs. Reprinted with permission from Ref. 28. © 2013 American Chemical Society.

replacing the high-temperature sintered TiO_2 compact layer with the hydrothermal synthesized TiO_2-NPs/graphene nanocomposite to fabricate the all low-temperature MSSCs,[34] which only needed 150 °C annealing temperature to form a dense TiO_2 ETL. The device has the structure: FTO/TiO_2-NPs-graphene/Al_2O_3 nanostructure/perovskite/spiro-OMeTAD/Au. Because of the excellent conductivity of graphene, this all low-temperature perovskite solar cell exhibits better charge collection efficiency than the devices with high-temperature sintered TiO_2 compact layer. Impedance analysis shows this n-type nanocomposite can significantly reduce the series resistance but increases the recombination resistance of device. As a result, the nanocomposite effectively improves the current density and fill factor to achieve the PCE of 16.6%.

Snaith et al. also synthesized TiO_2-NPs by a non-hydrolytic sol–gel route to replace the high-temperature sintered TiO_2 compact layer.[26] The TiO_2-NPs are dissolved into ethanol solution containing a small amount of titanium diisopropoxide bis(acetylacetonate) (TiAcAc) and spin-coated on a FTO substrate. TiAcAc decomposes to bridge the gaps of TiO_2-NPs during the heat annealing at 150 °C and form a compact layer, as shown in Figs. 3(a) and 3(b). The TiO_2-NPs layer shows a crack-less coverage with 100 fold higher conductivity than the high-temperature sintered TiO_2 compact layer. The increase of conductivity decreases the depletion width at the interface of FTO and TiO_2-NPs layer. A lower series resistance of device is also achieved when the depletion width decreases. This all low-temperature processed MSSCs can achieve a PCE of 15.9%.

In a short summary, both Al_2O_3-NPs mesoporous scaffold and TiO_2 compact layer can be fabricated at 150 °C to demonstrate a high efficiency low-temperature solution

Table II. Summary of electron transport layer fabrication temperature and the corresponding device performance in planar heterojunction perovskite solar cells.

Temperature (°C)	Process	Device structure	V_{oc} (V)	J_{sc} (mA/cm^2)	FF (%)	PCE (%)	Ref.
500	Spin-coating	FTO/ht-TiO_2/$CH_3NH_3PbI_{3-x}Cl_x$/spiro-OMeTAD/Au	0.98	22.9	0.69	15.4	38
500	Spin-coating	FTO/ht-TiO_2/$CH_3NH_3PbI_{3-x}Cl_x$/DR3TBDTT/Au	0.95	15.3	0.61	8.8	41
500	Spin-coating	FTO/MgO coated c-TiO_2/$CH_3NH_3PbI_3$/spiro-OMeTAD/Au	0.89	20.0	0.71	12.7	39
500	Spin-coating	FTO/ht-TiO_2/$HC(NH_2)_2PbI_3$/spiro-OMeTAD/Au	0.94	23.3	0.65	14.2	21
500	Spin-coating	ITO/ht-TiO_2/$CH_3NH_3PbI_{3-x}Cl_x$/P3HT/Ag	0.92	20.8	0.54	10.4	37
450	Pyrolysis spray	FTO/ht-TiO_2/$CH_3NH_3PbI_{3-x}Cl_x$/spiro-OMeTAD/Au	1.05	22.0	0.74	17.0	40
450	Spin-coating	FTO/ht-TiO_2/$CH_3NH_3PbI_{3-x}Cl_x$/CuSCN/Au	0.73	14.4	0.62	6.4	36
290	Spin-coating	ITO/ZnO/PCBM/$CH_3NH_3PbI_3$/PTB7-Th/MoO_3/Ag	1.00	18.2	0.67	12.2	46
200	Spin-coating	ITO/SnO_2/$CH_3NH_3PbI_3$/spiro-OMeTAD/Ag	1.08	19.5	0.62	13.0	47
160	Spin-coating	ITO/ZnO/C_3SAM/$CH_3NH_3PbI_3$/spiro-OMeTAD/MoO_3/Ag	1.07	22.5	0.65	15.7	43
150	Electrochemical deposition	ITO/ZnO/$CH_3NH_3PbI_3$/spiro-OMeTAD/Ag	0.91	22.6	0.53	10.9	45
150	Spin-coating	IZO/TiO_2-NPs/$CH_3NH_3PbI_3$/spiro-OMeTAD/Ag	1.02	16.8	0.71	12.2	48
150	Spin-coating	FTO/TiO_2-NPs/$CH_3NH_3PbI_{3-x}Cl_x$/spiro-OMeTAD/Au	0.98	21.0	0.69	14.2	49
150	Spin-coating	FTO/Y-doped TiO_2-NPs/$CH_3NH_3PbI_{3-x}Cl_x$/spiro-OMeTAD/Au	1.13	22.8	0.75	19.3	27
150	Spin-coating	FTO/WO_x/$CH_3NH_3PbI_{3-x}Cl_x$/spiro-OMeTAD/Ag	0.71	21.8	0.58	9.0	50
140	Spin-coating	ITO/CdSe-QDs[b]/$CH_3NH_3PbI_3$/spiro-OMeTAD/Ag	0.99	17.4	0.68	11.7	51
100	Chemical bath	FTO/Rutile TiO_2/$CH_3NH_3PbI_3$/spiro-OMeTAD/Au	1.05	19.8	0.64	13.7	42
100	Spin-coating	FTO/PEI/PCBM/$CH_3NH_3PbI_3$/PTAA/Au	1.03	20.3	0.72	15.2	52
Annealing free	Spin-coating	ITO/ZnO/$CH_3NH_3PbI_3$/spiro-OMeTAD/Ag	1.03	20.4	0.75	15.7	44

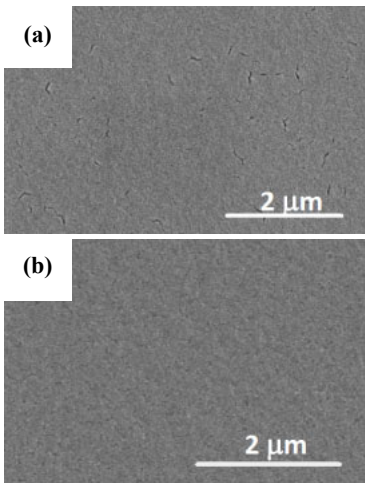

Fig. 3. (Color online) Top view SEM image for the surface of (a) TiO_2-NPs layer without TiAcAc; (b) TiO_2-NPs layer with 20% TiAcAc. Reprinted with permission from Ref. 26. © 2014 Royal Society of Chemistry.

processable MSSC. The high-temperature sintered TiO_2 compact layer can be substituted by the low-temperature processed TiO_2-NPs or graphene-TiO_2-NPs nanocomposite as a highly conductive and dense ETL. The high PCE of over 16% indicates that the MSSCs are quite appropriate to be fabricated by the all low-temperature process.

2.2 Low-temperature processed planar heterojunction perovskite solar cells

In order to simplify the complicated process of fabricating the mesoporous layer, many research groups endeavor to develop the PHJ perovskite solar cells. Some metal oxide nanoparticles, like TiO_2-NPs and ZnO-NPs, are adopted as the electron transport material because they are low-temperature solution processable, comparable energy level alignment and appropriated conductivity. We summarize the ETL fabrication temperature and the corresponding device performance of the state of the art PHJ perovskite solar cells in the Table II.

TiO_2-NPs thin film is a material of choices for a low-temperature processed electron transport layer. Yang et al. demonstrated the use of Y-doped anatase TiO_2-NPs as electron transport material for the fabrication of perovskite solar cell. The conductivity of Y-doped TiO_2-NPs is increased by one order than the pristine one. In addition, transient photocurrent measurement shows the improvement of carrier transport in the device. The faster photocurrent decay is exhibited in the Y-doping based devices than the reference ones. The result is consistent with PL measurement which indicates a 30% less decay time of perovskite layer on Y-doped TiO_2-NPs, as shown in Fig. 4(a). The enhanced electron transport and collection efficiency of Y-doped TiO_2-NPs significantly improves the current performance [Fig. 4(b)]. With other optimized processing conditions, the champion device can be obtained with a PCE of 19.3%. This work shows that the high-temperature sintered compact TiO_2 layer[21,35–41] in PHJ perovskite solar cell can be successfully replaced by the low-temperature TiO_2-NPs layer. Thus, the highest PCE device is achievable using the low-temperature processed ETL.[27,42–52]

Except for the TiO_2-NPs, Graztel et al. used a chemical bath deposition method to grow the rutile TiO_2 nanocrystalline as electron transport material on FTO substrate.[42] The growth of rutile TiO_2 was prepared only at 70 °C by controlling the concentration of $TiCl_4$. An intimate junction of large interfacial area between TiO_2 and perovskite material is observed. The intimate junction facilitates the extracting of electron from the perovskite layer. The PCE of rutile TiO_2-based device can be improved from 3.7 to 13.7%.

On the other hand, due to the comparable energy levels and superior electron conductivity, ZnO is widely used as an

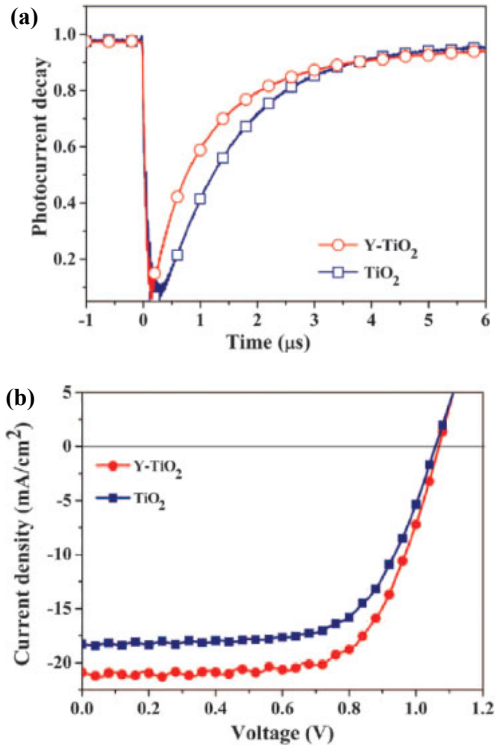

Fig. 4. (Color online) (a) Photocurrent decay measurement of perovskite layer on pristine TiO_2-NPs layer and Y-TiO_2-NPs layer. (b) *J–V* curve of perovskite solar cell based on pristine TiO_2-NPs layer and Y-TiO_2-NPs electron transport material. Reprinted with permission from Ref. 27. © 2014 AAAS.

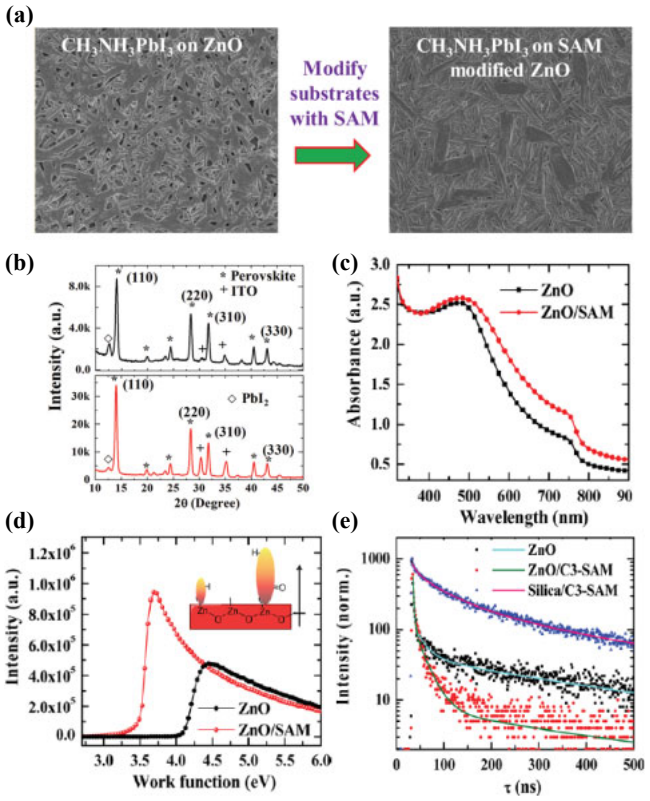

Fig. 5. (Color online) (a) Morphology change of perovskite layer on the C3-SAM modified ZnO. (b) XRD patterns of perovskite layer on ZnO/C3-SAM (black line) and ZnO (red line). (c) Light absorption spectrum of perovskite layer on ZnO/C3-SAM and ZnO. (d) Lowered work function of perovskite layer on ZnO. (e) Faster PL quench of perovskite layer on ZnO/C3-SAM. Reprinted with permission from Ref. 43. © 2015 American Chemical Society.

alternative n-type material for high-temperature sintered TiO_2. For the conventional sol–gel method to prepare ZnO layer, the high-temperature sintering process is required. Chen et al. developed a new way to prepare the sol–gel ZnO layer on ITO substrate without sintering.[43] Meanwhile, they modified the surface by 3-aminopropanioc acid self-assembling monolayer (C_3-SAM) to fill the pinholes of ZnO layer to improve the morphology of perovskite layer, as shown in Fig. 5(a). From the X-ray diffraction (XRD) patterns, the more complete conversion of PbI_2 to perovskite material is observed on the modified ZnO compact layer [Fig. 5(b)]. Therefore, the light absorption of perovskite layer increases [Fig. 5(c)]. Besides, the permanent dipole moments of C_3-SAM can lower the work function of ZnO from 4.17 to 3.52 eV [Fig. 5(d)]. The energy level of ZnO becomes more compatible to the lowest unoccupied molecular orbital (LUMO) of perovskite layer. As a result, a better energy band alignment facilitates the carrier extraction and charge generation. In addition, the PL measurement also shows reduced trap states and strengthened electron coupling of perovskite layer [Fig. 5(e)]. The suppressed charge recombination and faster charge collection rate are achieved by the C_3-SAM modification. It provides an effective strategy to improve the short circuit current density (J_{sc}) from 19.12 to 22.51 mA/cm^2 and the PCE from 11.96 to 15.67%, respectively.

Kelly et al. adopted the ZnO-NPs as electron transport material to fabricate the PHJ perovskite solar cell.[44] The ZnO-NPs were synthesized by the hydrolysis of zinc acetate in methanol and spin-coated on ITO to form a uniform thin film without heat annealing. The advantages of this kind of ZnO-NPs are the elimination of high-temperature sintering process and the achievement of higher electron mobility than that of TiO_2. The perovskite layer was deposited on the ZnO-NPs layer by the sequential deposition method. By this annealing free ZnO-NPs ETL, the device can be fabricated by a complete low-temperature solution process. The PCE of the device successfully reaches to 15.7% on the glass/ITO substrate and 10.2% on the PET/ITO substrate.

Except the common spin-coating method, Pauporte et al. fabricated an 11% PCE device with a fast-prepared ZnO layer by an electrochemical technique.[45] The ZnO layer is directly deposited on the ITO by a three-electrode cell in a $Zn(NO_3)_2$ solution. By this novel deposition method of ETL, the time required for preparing the ZnO layer can be significantly decreased to a short time of 2 min at 60 °C.

In a short summary, the metal oxides such as ZnO and TiO_2 provide promising and efficient electron transport materials to fabricate the PHJ perovskite solar cells at low temperature. By decreasing the fabrication temperature of ETL, the damage of flexible substrate can be avoided. These developments promote the advancement of perovskite solar cells toward the large scale production by roll-to-roll technique.

3. Conclusions

We systemically review the state of the art of low-temperature solution processed electron transport layer of the n–i–p perovskite solar cells. The TiO_2-NPs/graphene nanocomposite, nonhydrolytic and sol–gel route synthesized TiO_2-NPs

are successfully demonstrated that they can replace the high-temperature sintered compact TiO_2 as electron transport material in the MSSCs. For the PHJ perovskite solar cell, an extremely high PCE of 19.3% is achieved with the low-temperature prepared Y-doped TiO_2-NPs electron transport material. The material has enhanced conductivity and reduced series resistance. On the other hand, ZnO is another good electron transport material because of the comparable energy level alignment and good conductivity. The PHJ perovskite solar cells with ZnO-NPs or sol–gel prepared ZnO ETL can achieve the PCE over 15%.

For the commercialization of perovskite solar cells, the roll-to-roll process is a convenient and cost-effective way to scale up the fabrication of devices. The high-temperature process is not suitable for the fabrication on flexible substrate. As a result, the development of low-temperature solution processes is very critical. So far, scientists have successfully demonstrated that the low-temperature solution processing perovskite solar cells could perform high efficiency on rigid substrate. It implied that the perovskite solar cell has high potential to fabricate on the flexible substrate. Further developments are still required to achieve the fabrication of the flexible solar cells.

Acknowledgement

Financial support obtained from the National Science Council of Taiwan (MOST 104-3113-E-002-010) for this research is highly appreciated.

1) D. H. Cao, C. C. Stoumpos, O. K. Farha, J. T. Hupp, and M. G. Kanatzidis, J. Am. Chem. Soc. **137**, 7843 (2015).
2) F. Hao, C. C. Stoumpos, D. H. Cao, R. P. H. Chang, and M. G. Kanatzidis, Nat. Photonics **8**, 489 (2014).
3) F. Hao, C. C. Stoumpos, R. P. Chang, and M. G. Kanatzidis, J. Am. Chem. Soc. **136**, 8094 (2014).
4) N. J. Jeon, J. H. Noh, W. S. Yang, Y. C. Kim, S. Ryu, J. Seo, and S. I. Seok, Nature **517**, 476 (2015).
5) M. H. Kumar, S. Dharani, W. L. Leong, P. P. Boix, R. R. Prabhakar, T. Baikie, C. Shi, H. Ding, R. Ramesh, M. Asta, M. Graetzel, S. G. Mhaisalkar, and N. Mathews, Adv. Mater. **26**, 7122 (2014).
6) J. H. Noh, S. H. Im, J. H. Heo, T. N. Mandal, and S. I. Seok, Nano Lett. **13**, 1764 (2013).
7) Y. Ogomi, A. Morita, S. Tsukamoto, T. Saitho, N. Fujikawa, Q. Shen, T. Toyoda, K. Yoshino, S. S. Pandey, T. Ma, and S. Hayase, J. Phys. Chem. Lett. **5**, 1004 (2014).
8) B.-W. Park, B. Philippe, X. Zhang, H. Rensmo, G. Boschloo, and E. M. J. Johansson, Adv. Mater. **27**, 6806 (2015).
9) D. Sabba, H. K. Mulmudi, R. R. Prabhakar, T. Krishnamoorthy, T. Baikie, P. P. Boix, S. Mhaisalkar, and N. Mathews, J. Phys. Chem. C **119**, 1763 (2015).
10) L. Zheng, Y. Ma, S. Chu, S. Wang, B. Qu, L. Xiao, Z. Chen, Q. Gong, Z. Wu, and X. Hou, Nanoscale **6**, 8171 (2014).
11) Y. Zhou, M. Yang, W. Wu, A. L. Vasiliev, K. Zhu, and N. P. Padture, J. Mater. Chem. A **3**, 8178 (2015).
12) S. De Wolf, J. Holovsky, S. J. Moon, P. Loper, B. Niesen, M. Ledinsky, F. J. Haug, J. H. Yum, and C. Ballif, J. Phys. Chem. Lett. **5**, 1035 (2014).
13) M. A. Green, A. Ho-Baillie, and H. J. Snaith, Nat. Photonics **8**, 506 (2014).
14) E. T. Hoke, D. J. Slotcavage, E. R. Dohner, A. R. Bowring, H. I. Karunadasa, and M. D. McGehee, Chem. Sci. **6**, 613 (2015).
15) J. W. Lee, D. J. Seol, A. N. Cho, and N. G. Park, Adv. Mater. **26**, 4991 (2014).
16) J. Qiu, Y. Qiu, K. Yan, M. Zhong, C. Mu, H. Yan, and S. Yang, Nanoscale **5**, 3245 (2013).
17) C. Wehrenfennig, M. Liu, H. J. Snaith, M. B. Johnston, and L. M. Herz, J. Phys. Chem. Lett. **5**, 1300 (2014).
18) W. J. Yin, T. Shi, and Y. Yan, Adv. Mater. **26**, 4653 (2014).
19) W. S. Yang, J. H. Noh, N. J. Jeon, Y. C. Kim, S. Ryu, J. Seo, and S. I. Seok, Science **348**, 1234 (2015).
20) S. D. Stranks, G. E. Eperon, G. Grancini, C. Menelaou, M. J. P. Alcocer, T. Leijtens, L. M. Herz, A. Petrozza, and H. J. Snaith, Science **342**, 341 (2013).
21) G. E. Eperon, S. D. Stranks, C. Menelaou, M. B. Johnston, L. M. Herz, and H. J. Snaith, Energy Environ. Sci. **7**, 982 (2014).
22) A. Kojima, K. Teshima, Y. Shirai, and T. Miyasaka, J. Am. Chem. Soc. **131**, 6050 (2009).
23) J. H. Im, C. R. Lee, J. W. Lee, S. W. Park, and N. G. Park, Nanoscale **3**, 4088 (2011).
24) H.-S. Kim, C.-R. Lee, J.-H. Im, K.-B. Lee, T. Moehl, A. Marchioro, S.-J. Moon, R. Humphry-Baker, J.-H. Yum, J. E. Moser, M. Grätzel, and N.-G. Park, Sci. Rep. **2**, 591 (2012).
25) M. M. Lee, J. Teuscher, T. Miyasaka, T. N. Murakami, and H. J. Snaith, Science **338**, 643 (2012).
26) K. Wojciechowski, M. Saliba, T. Leijtens, A. Abateand, and H. J. Snaith, Energy Environ. Sci. **7**, 1142 (2014).
27) H. Zhou, Q. Chen, G. Li, S. Luo, T. B. Song, H. S. Duan, Z. Hong, J. You, Y. Liu, and Y. Yang, Science **345**, 542 (2014).
28) W. Zhang, M. Saliba, S. D. Stranks, Y. Sun, X. Shi, U. Wiesner, and H. J. Snaith, Nano Lett. **13**, 4505 (2013).
29) E. Edri, S. Kirmayer, M. Kulbak, G. Hodes, and D. Cahen, J. Phys. Chem. Lett. **5**, 429 (2014).
30) E. Edri, S. Kirmayer, D. Cahen, and G. Hodes, J. Phys. Chem. Lett. **4**, 897 (2013).
31) S. N. Habisreutinger, T. Leijtens, G. E. Eperon, S. D. Stranks, R. J. Nicholas, and H. J. Snaith, Nano Lett. **14**, 5561 (2014).
32) A. Abate, D. J. Hollman, J. Teuscher, S. Pathak, R. Avolio, G. D'Errico, G. Vitiello, S. Fantacci, and H. J. Snaith, J. Am. Chem. Soc. **135**, 13538 (2013).
33) J. M. Ball, M. M. Lee, A. Hey, and H. J. Snaith, Energy Environ. Sci. **6**, 1739 (2013).
34) J. T.-W. Wang, J. M. Ball, E. M. Barea, A. Abate, J. A. Alexander-Webber, J. Huang, M. Saliba, I. Mora-Sero, J. Bisquert, H. J. Snaith, and R. J. Nicholas, Nano Lett. **14**, 724 (2014).
35) K. Wojciechowski, S. D. Stranks, A. Abate, G. Sadoughi, A. Sadhanala, N. Kopidakis, G. Rumbles, C.-Z. Li, R. H. Friend, A. K.-Y. Jen, and H. J. Snaith, ACS Nano **8**, 12701 (2014).
36) S. Chavhan, O. Miguel, H.-J. Grande, V. Gonzalez-Pedro, R. S. Sánchez, E. M. Barea, I. Mora-Seró, and R. Tena-Zaera, J. Mater. Chem. A **2**, 12754 (2014).
37) B. Conings, L. Baeten, C. De Dobbelaere, J. D'Haen, J. Manca, and H. G. Boyen, Adv. Mater. **26**, 2041 (2014).
38) P. Docampo, F. C. Hanusch, S. D. Stranks, M. Döblinger, J. M. Feckl, M. Ehrensperger, N. K. Minar, M. B. Johnston, H. J. Snaith, and T. Bein, Adv. Energy Mater. **4**, 1400355 (2014).
39) G. S. Han, H. S. Chung, B. J. Kim, D. H. Kim, J. W. Lee, B. S. Swain, K. Mahmood, J. S. Yoo, N.-G. Park, J. H. Lee, and H. S. Jung, J. Mater. Chem. A **3**, 9160 (2015).
40) F. Huang, Y. Dkhissi, W. Huang, M. Xiao, I. Benesperi, S. Rubanov, Y. Zhu, X. Lin, L. Jiang, Y. Zhou, A. Gray-Weale, J. Etheridge, C. R. McNeill, R. A. Caruso, U. Bach, L. Spiccia, and Y.-B. Cheng, Nano Energy **10**, 10 (2014).
41) L. Zheng, Y. H. Chung, Y. Ma, L. Zhang, L. Xiao, Z. Chen, S. Wang, B. Qu, and Q. Gong, Chem. Commun. **50**, 11196 (2014).
42) A. Yella, L. P. Heiniger, P. Gao, M. K. Nazeeruddin, and M. Gratzel, Nano Lett. **14**, 2591 (2014).
43) L. Zuo, Z. Gu, T. Ye, W. Fu, G. Wu, H. Li, and H. Chen, J. Am. Chem. Soc. **137**, 2674 (2015).
44) D. Liu and T. L. Kelly, Nat. Photonics **8**, 133 (2014).
45) J. Zhang, E. J. Juárez-Pérez, I. Mora-Seró, B. Viana, and T. Pauporté, J. Mater. Chem. A **3**, 4909 (2015).
46) J. Kim, G. Kim, T. K. Kim, S. Kwon, H. Back, J. Lee, S. H. Lee, H. Kang, and K. Lee, J. Mater. Chem. A **2**, 17291 (2014).
47) J. Song, E. Zheng, J. Bian, X.-F. Wang, W. Tian, Y. Sanehira, and T. Miyasaka, J. Mater. Chem. A **3**, 10837 (2015).
48) Y. Dkhissi, F. Huang, S. Rubanov, M. Xiao, U. Bach, L. Spiccia, R. A. Caruso, and Y.-B. Cheng, J. Power Sources **278**, 325 (2015).
49) C. Y. Chang, C. Y. Chu, Y. C. Huang, C. W. Huang, S. Y. Chang, C. A. Chen, C. Y. Chao, and W. F. Su, ACS Appl. Mater. Interfaces **7**, 4955 (2015).
50) K. Wang, Y. Shi, Q. Dong, Y. Li, S. Wang, X. Yu, M. Wu, and T. Ma, J. Phys. Chem. Lett. **6**, 755 (2015).
51) L. Wang, W. Fu, Z. Gu, C. Fan, X. Yang, H. Li, and H. Chen, J. Mater. Chem. C **2**, 9087 (2014).
52) S. Ryu, J. Seo, S. S. Shin, Y. C. Kim, N. J. Jeon, J. H. Noh, and S. I. Seok, J. Mater. Chem. A **3**, 3271 (2015).